AIAA JOURNAL
Vol. 37, No. 12, December 1999

Jet Characteristics of a Plunging Airfoil

J. C. S. Lai* and M. F. Platzer†
Naval Postgraduate School, Monterey, California 93943-5106

Water-tunnel tests of a NACA 0012 airfoil that was oscillated sinusoidally in plunge are described. The flowfield downstream of the airfoil was explored by dye flow visualization and single-component laser Doppler velocimetry (LDV) measurements for a range of freestream speeds, frequencies, and amplitudes of oscillation. The dye visualizations show that the vortex patterns generated by the plunging airfoil change from drag-producing wake flows to thrust-producing jet flows as soon as the ratio of maximum plunge velocity to freestream speed, i.e., the nondimensional plunge velocity, exceeds approximately 0.4. The LDV measurements show that the nondimensional plunge velocity is the appropriate parameter to collapse the maximum streamwise velocity data covering a nondimensional plunge velocity range from 0.18 to 9.3. The maximum streamwise velocity at a given streamwise distance downstream starts to exceed the freestream speed as soon as the nondimensional plunge velocity exceeds 0.25. Furthermore, this maximum jet velocity has been shown to be a linear function of the nondimensional plunge velocity.

Nomenclature

a_p	= amplitude of oscillation
b	= averaged jet half width
C_t	= thrust coefficient, $T/(\frac{1}{2}\rho_0 U_0^2 c)$
c	= chord
f	= frequency of oscillation, Hz
h	= nondimensional amplitude of oscillation, a_p/c
k	= reduced frequency parameter, $=2\pi f c/U_0$
kh	= nondimensional plunge velocity, $=2\pi f a_p/U_0$
T	= thrust per unit span
U	= mean (time-averaged) streamwise velocity
$U_{\max}$	= maximum mean streamwise velocity
U_0	= freestream velocity
x	= streamwise direction measured from the trailing edge of the airfoil
y	= lateral direction measured from the center line of the airfoil
$y_{\max}$	= location in the lateral direction where $U = U_{\max}$ at a given x
ρ_0	= freestream density

I. Introduction

An early analysis of oscillating airfoils was made by Birnbaum[1] in the early 1920s using a low-frequency expansion to the fourth power, and his results are only valid for relatively small reduced-frequency values. Birnbaum[1] also gave an analytical expression for the thrust generated by sinusoidal plunge oscillation of the airfoil. In the 1930s Theodorsen[2] gave a theory for the same problem, which is valid for any frequency within the limitations of small amplitude oscillations in inviscid incompressible flow. These and many subsequent studies were motivated by the need to predict the onset of aircraft wing flutter. Experimental verification of the flutter prediction was mostly accomplished by measuring the flutter speed, and relatively little experimental information is available about the precise fluid physics of oscillating airfoils.

With some exceptions, such as Ho and Chen,[3] Ahmed and Chandrasekhara,[4] Panda and Zaman,[5] and Oshima and Ramaprian,[6] most of the experimental studies were made with flow visualization or pressure measurements. Recently, Ahmed and Chandrasekhara[4] applied two-component laser Doppler velocimetry (LDV) to study the reattachment process of dynamic stall flow over an oscillating airfoil while Panda and Zaman's X-wire measurements[5] covered the wake of an oscillating airfoil up to two chord lengths downstream. More recently, Oshima and Ramaprian[6] applied particle image velocimetry (PIV) to study the dynamic stall vortex caused by a pitching airfoil in a water tunnel. Koochesfahani[7] has demonstrated that the effect of oscillating an airfoil in pitch on the mean flow is much more dramatic than acoustic excitation effects observed in free shear layers. His flow visualization and LDV results have shown that oscillating an airfoil at certain frequencies and amplitudes can transform a wake profile with velocity defect into a jet profile with velocity excess, resulting in thrust rather than drag. On the other hand, the mean flow in free shear layers generally retains its shape under acoustic excitation.

Whereas an airfoil oscillating about a pivot results in different angles of incidence at different phases of the oscillation, a plunging airfoil is one in which the airfoil is displaced periodically in the vertical direction with its orientation fixed relative to a fixed frame of reference. Knoller,[8] and later independently Betz,[9] recognized that a plunging airfoil generates thrust. This Knoller–Betz effect was verified experimentally by Katzmayr.[10] Based on flat-plate airfoil theory, Garrick[11] showed that the propulsive efficiency of plunging airfoils drops rapidly from values close to one at very low flapping frequencies to close to 0.5 as the frequency is increased. On the other hand, Schmidt[12] demonstrated that with a tandem arrangement in which a stationary airfoil was positioned in the wake of a plunging airfoil, the propulsive efficiency could be doubled. This was later given a theoretical foundation by Bosch[13] using a small amplitude, linear inviscid incompressible flow analysis for two interfering oscillating plates. Recently, Dohring et al.[14] showed both experimentally and computationally that when an airfoil is oscillated in plunge with an appropriate combination of frequency and amplitude, a jet (instead of wake) is produced downstream of the trailing edge. The jet entrainment characteristics resulting from a plunging airfoil have been exploited by Lai et al.[15] to control the reattachment of a backward facing step flow.

Flows around oscillating airfoils are relevant for the analysis of aircraft wing flutter, helicopter and turbomachine blade flutter, and for the prediction of the aeroacoustic noise generation. However, they have also attracted significant attention in biohydrodynamics because of the need to understand the propulsion mechanisms of

Presented as Paper 98-0101 at the AIAA 36th Aerospace Sciences Meeting, Reno, NV, 12–15 January 1998; received 20 February 1998; revision received 1 December 1998; accepted for publication 4 April 1999.

*National Research Council Senior Research Associate, Department of Aeronautics and Astronautics; on leave from School of Aerospace and Mechanical Engineering, University College, Australian Defence Force Academy, University of New South Wales, Canberra, Australian Capital Territory 2600, Australia. Senior Member AIAA.

†Distinguished Professor, Department of Aeronautics and Astronautics. Associate Fellow AIAA.

aquatic animals, birds, and insects. Lighthill[16] applied the slender-body theory to study the swimming of a slender fish, whereas Wu[17] applied potential flow theory to a waving plate (considered as a two-dimensional flat fish). By extending the unsteady lifting-surface theory with a quasicontinuous loading approach, Lan[18] was able to calculate propulsive efficiency and thrust for some swept and rectangular planforms undergoing combined pitching (oscillating in pitch) and heaving (pure plunging) motions. By applying the vortex ring panel method, Cheng et al.[19] explored the swimming performance of fish undulatory motion using three-dimensional waving plates. Through a linear instability analysis Triantafyllou et al.[20] deduced that maximum thrust per unit input energy in oscillating an airfoil occurs in the range of Strouhal number St between 0.25 and 0.35. Here Strouhal number is defined as fA/V, where A is the width of the wake, taken to be equal to the maximum excursion of the foil's trailing edge (double amplitude), and V is the average forward velocity. Their experiments of measuring the force acting on a NACA 0012 airfoil undergoing both pitching and plunging motions and data from observations on fish and cetaceans appear to confirm this Strouhal number range. More recently, Anderson et al.[21] conducted force and power measurements of oscillating foils. They found that optimal production of thrust occurs at $St = 0.25$–0.40, large amplitude of heave motion-to-chord ratio (of order one), large maximum angle of attack (between 15 and 25 deg), and a phase angle between heave and pitch of about 75 deg. Furthermore, their flow visualization using digital PIV indicates that conditions of high efficiency for thrust production are associated with the interaction of a moderately strong leading-edge vortex with the trailing-edge vorticity.

Although the wake vortex patterns behind airfoils undergoing small amplitude pitching oscillations have been studied quite extensively (see, for example, Ref. 7), wakes behind purely plunging airfoils have not received as much attention until recently. Freymuth[22] demonstrated thrust production for plunging airfoils using flow visualization. Preliminary flow visualization and LDV studies made at the Naval Postgraduate School (NPS) by Jones et al.[23] and by Dohring[24] have enabled the excitation to be classified as drag producing, neutral, or thrust producing in terms of the excitation frequency and amplitude. Nevertheless, more detailed quantitative measurements of the jet characteristics of a plunging airfoil are hitherto unavailable in the literature. The objective of this study is primarily directed at quantifying and understanding the jet characteristics of a plunging airfoil as a function of the plunging frequency and amplitude and the freestream velocity.

II. Experimental Setup and Instrumentation

All of the experiments reported here were conducted in the water tunnel facility at the Department of Aeronautics and Astronautics, NPS. The water tunnel is a closed-circuit, continuous-flow facility with a contraction ratio of 6:1. The test section is 380 mm wide, 1500 mm long, and 510 mm high. Side walls and the bottom of the test section as well as the end wall are made of glass to provide optical access for flow visualization and LDV measurements. The top of the test section is open to atmosphere. The flow velocity can be adjusted in a range from 0 to about 0.5 m/s.

Experiments were conducted using two NACA 0012 airfoils with a span of 370 mm including the end supports. The larger airfoil with a chord c of 100 mm was primarily used for measurements in the near field close to the trailing edge while the smaller airfoil with a chord c of 10 mm was used for measurements in the far field. A Model 113 Elektro-seis shaker from APS Dynamics, Inc., driven by an APS Model 114 amplifier was mounted on top of the test section to oscillate the airfoil sinusoidally in plunge. The signal from a Wavetek 115 frequency generator was varied from 2.5 to 10 Hz. The amplitude of oscillation, measured with a Lucas DC-E500 DC-operated linear variable displacement transducer, was varied primarily from 2.5 to 6 mm. Experiments were mainly conducted for freestream velocities of 0.05, 0.11, and 0.21 m/s corresponding to a Reynolds number range of 500–2.1×10^4 based on chord.

A Thermal Systems, Inc. (TSI), single-component LDV was used to measure the mean streamwise velocity and streamwise turbulence intensity distributions up to 30 chord lengths downstream of the trailing edge of the airfoil. The fiber-optic probe head could be traversed with an accuracy of 0.1 mm in the streamwise x, transverse y, and spanwise z directions using a Lintech Model 41583 traverse table driven by Applied Motion Products 1618 power supply and interface. The light source was an Omnichrome Model 543-300A argon ion laser with a rated output of 300 mW at 8.8 A. The beam separation was 50 mm, and the focal length was 350 mm, giving a fringe spacing of 3.427 μm for the blue beam. The Doppler signal was processed with a TSI IFA 550 intelligent flow processor. The data acquisition was automated using a Pentium 150 MHz PC and TSI Flow information display (FIND) software version 4.5. At least 1000 data samples were used for each measurement point. Although the maximum differences between corrected and uncorrected data were less than 2%, velocity correction based on time between data was applied. Uncertainty estimates indicate that the uncertainty in the mean velocity measurements is within ± 5 mm/s. For the 10-mm chord airfoil LDV measurements were made at 10 streamwise stations measured from the trailing edge, namely, $x/c = -2.8$, 1.8, 2.5, 3, 4, 5, 7.5, 10, 15, and 20. For each streamwise station a nonuniform grid in the transverse direction consisting of a minimum of 29 points was used to cover y/c from -3.5 to 3.5, with more points concentrating in the high velocity gradient region. The smallest spacing between measurement points in the transverse direction was 1 mm. For the 100-mm chord airfoil measurements were made at six streamwise stations measured from the trailing edge, namely, $x/c = -1.2$, 0.5, 1, 1.8, 2.5, and 3. For each streamwise station a nonuniform grid in the transverse direction consisting of a minimum of 33 points was used to cover y/c from -0.9 to 0.9, with more points concentrating in the high velocity gradient region. The smallest spacing between measurement points in the transverse direction was 2 mm. All streamwise velocity measurements were made by the single component LDV in the midspan plane for a total of 54 combinations of freestream velocity, amplitude and frequencies of oscillation, and two different sizes of airfoil. The flow is assumed to be nominally two-dimensional. Dye flow visualization was also conducted in the midspan plane for a number of cases using the large airfoil. A red dye was injected through the upper surface close to the trailing edge while a green dye was injected through the lower surface close to the trailing edge.

III. Results

A. Flow Visualization

As shown by Jones et al.,[23] the wake structures behind a 10-mm chord NACA 0012 airfoil plunging sinusoidally at a relatively low kh (=0.29) consist of clockwise rotating vortices in the upper row and counterclockwise rotating vortices in the lower row, thus indicating drag. On the other hand, they showed that when the airfoil is oscillated in plunge at a sufficiently high kh (=0.6) the upper row of vortices are counterclockwise rotating while the lower row of vortices are clockwise rotating, thus indicative of thrust. Note that kh represents the maximum nondimensional plunge velocity. As shown in Fig. 1, LDV measurements of the mean streamwise velocity at $0.41c$ downstream of the trailing edge reveal a velocity defect (wake) for a stationary NACA 0012 airfoil and a jet with a

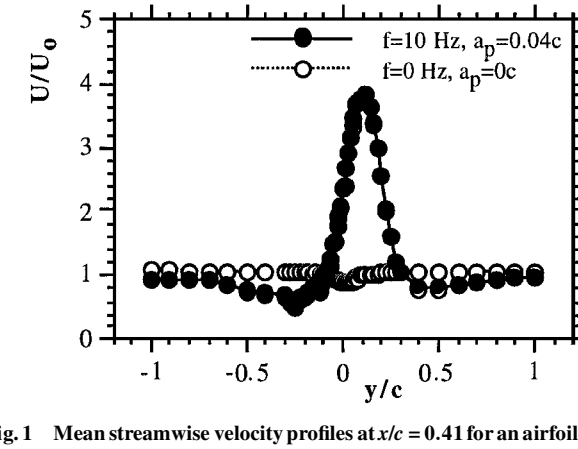

Fig. 1 Mean streamwise velocity profiles at $x/c = 0.41$ for an airfoil with and without flapping.

Fig. 2 Vortex patterns for a stationary NACA 0012 airfoil for a freestream velocity of 0.2 m/s.

maximum velocity of almost four times that of the freestream velocity when the airfoil is oscillated in plunge at $k = 48.3$ and $h = 0.04$ (i.e., $kh = 1.932$) for a freestream velocity of 0.13 m/s.

Flow visualization photos for various flow conditions were taken for a NACA 0012 airfoil with a chord of 100 mm. Figure 2 shows the typical Kármán vortex street behind the stationary airfoil for a freestream velocity of 0.2 m/s, in which clockwise rotating vortices (red) are shed from the upper surface and counterclockwiserotating vortices (green) are shed from the lower surface. Flow visualization photos depicted in Figs. 3–5 are for a plunging airfoil. These photos were taken with the same scale, and the backgroundhad been edited to provide a uniform color to highlight the salient features of the wake.

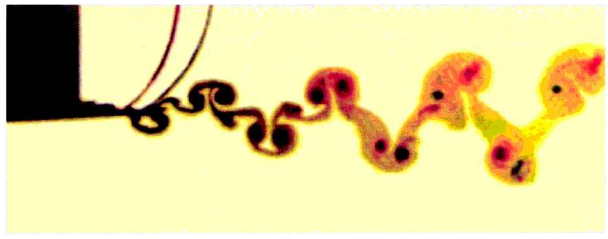

a) $h = 0.0125$ ($kh = 0.098$)

b) $h = 0.025$ ($kh = 0.196$)

c) $h = 0.05$ ($kh = 0.393$)

d) $h = 0.075$ ($kh = 0.589$)

e) $h = 0.1$ ($kh = 0.785$)

Fig. 3 Vortex patterns for a NACA 0012 airfoil oscillated in plunge for a freestream velocity of about 0.2 m/s, a frequency of $f = 2.5$ Hz ($k = 7.85$), and various amplitudes of oscillation.

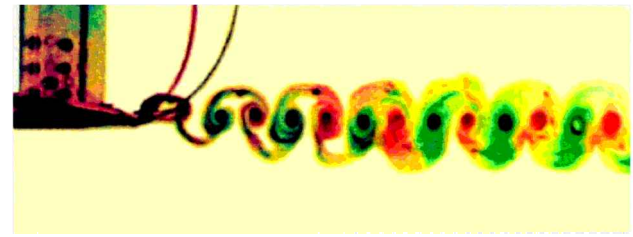

a) $h = 0.0125$ ($kh = 0.196$)

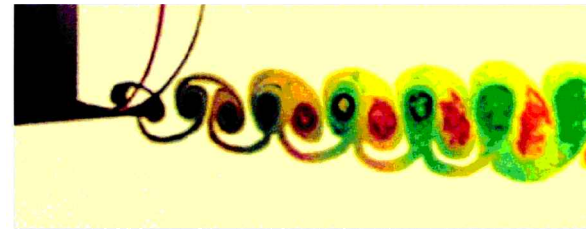

b) $h = 0.025$ ($kh = 0.393$)

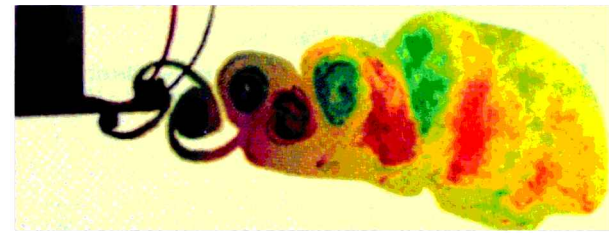

c) $h = 0.05$ ($kh = 0.785$)

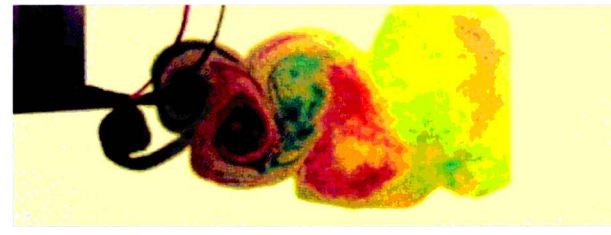

d) $h = 0.075$ ($kh = 1.178$)

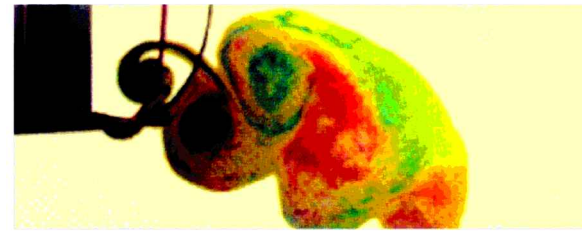

e) $h = 0.1$ ($kh = 1.570$)

Fig. 4 Vortex patterns for a NACA 0012 airfoil oscillated in plunge for a freestream velocity of about 0.2 m/s, a frequency of $f = 5$ Hz ($k = 15.7$), and various amplitudes of oscillation.

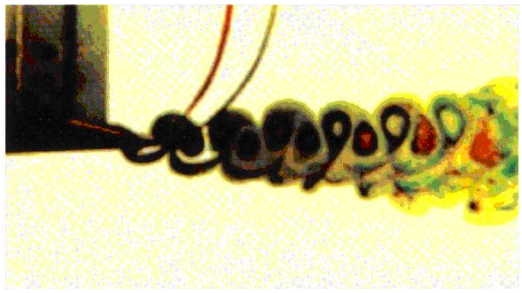

a) $h = 0.0125$ ($kh = 0.393$)

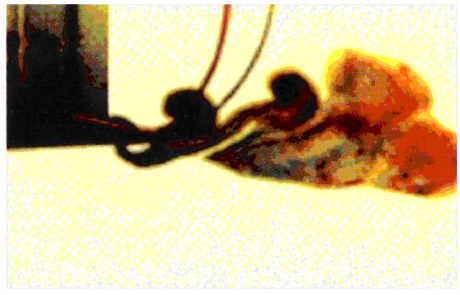

b) $h = 0.025$ ($kh = 0.785$)

c) $h = 0.05$ ($kh = 1.570$)

Fig. 5 Vortex patterns for a NACA 0012 airfoil oscillated in plunge for a freestream velocity of about 0.2 m/s, a frequency of $f = 10$ Hz ($k = 31.4$), and various amplitudes of oscillation.

Figures 3a–3e display the vortex patterns for a freestream velocity of about 0.2 m/s as the airfoil is oscillated in plunge at a frequency of 2.5 Hz ($k = 7.85$) for $h = 0.0125$, 0.025, 0.05, 0.075, and 0.1, respectively. These conditions correspond to a nondimensional plunge velocity kh of 0.098, 0.196, 0.393, 0.589, and 0.785, respectively. Figure 3a shows that, whereas the wake is indicative of drag, the mushroomlike vortices are changing their orientation from pointing upstream to almost pointing vertically upward or downward. As the amplitude h is further increased, Fig. 3b shows that vortices are not shed alternately one at a time from the upper and lower surfaces. Instead, two vortices of the same sign are shed from the same side before another two are shed from the opposite side. Furthermore, the mushroom-like vortices' orientation is now pointing slightly downstream. These patterns typify the transition from the drag-producing wake to a neutral wake. Sketches of the vortex shedding process for this condition extracted from flow visualization video are given in Fig. 6a. For kh greater than 0.4, Figs. 3c–3e shows that the upper row of vortices (green) are now counterclockwise rotating and the lower row of vortices (red) are clockwise rotating, thus indicating a jet-like flowfield and thrust production. Frame-by-frame analysis of the flow visualization video taken indicates that counterclockwise rotating vortices are shed from the lower surface when the airfoil reaches its top position (i.e., at $y = a_p$), whereas the clockwise rotating vortices are shed from the upper surface when the airfoil reaches its bottom position (i.e., at $y = -a_p$). Sketches depicting this vortex shedding process are given in Fig. 6b.

Figures 4a–4e display the vortex patterns for a freestream velocity of about 0.2 m/s as the airfoil is oscillated in plunge at a frequency of 5 Hz ($k = 15.7$) for $h = 0.0125$, 0.025, 0.05, 0.075, and 0.1, respectively. These conditions correspond to a nondimensional plunge velocity kh of 0.196, 0.393, 0.785, 1.178, and 1.570, respectively. For kh in the vicinity of 0.2, Fig. 4a shows that the behavior of the wake is almost neutral. For kh greater than 0.2, Figs. 4b–4e indicate that the resulting wake is definitely jetlike, as has already been observed for $f = 2.5$ Hz in Figs. 3c–3e.

Figures 5a–5c display the vortex patterns for a freestream velocity of about 0.2 m/s as the airfoil is oscillated in plunge at a frequency of 10 Hz ($k = 31.4$) for $h = 0.0125$, 0.025, and 0.05, respectively. These conditions correspond to a nondimensional plunge velocity kh of 0.393, 0.785, and 1.570, respectively. Whereas the vortex patterns are similar to those depicted for 2.5 and 5 Hz, they appear to be smaller for similar values of kh. Furthermore, the vortex street

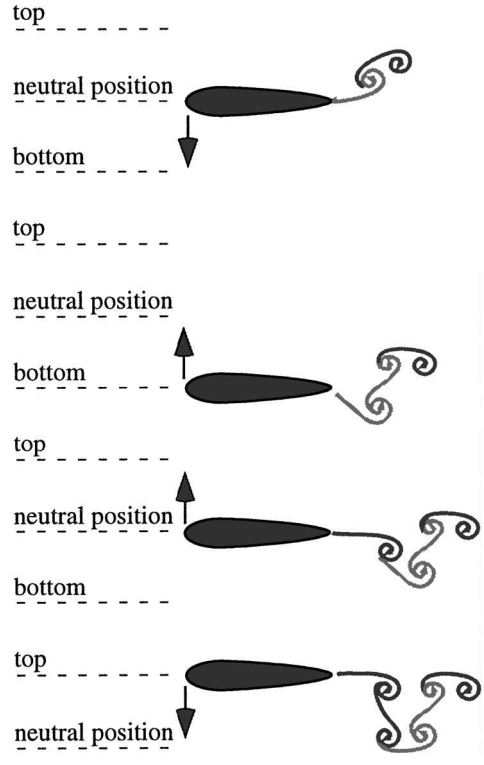

a) $kh \approx 0.2$

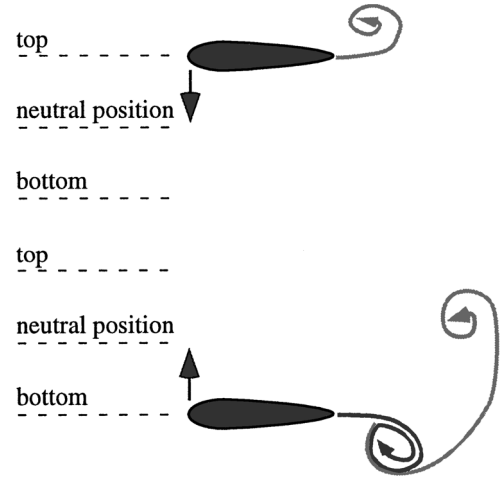

b) $kh \approx 0.6$

Fig. 6 Sketch of the vortex shedding process as the airfoil moves through various positions.

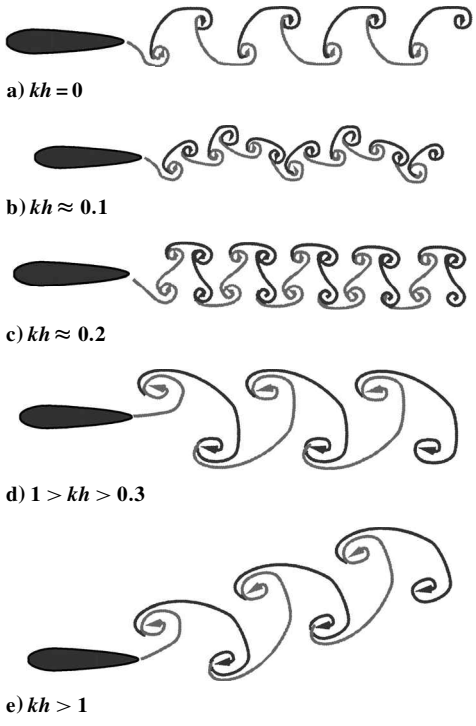

Fig. 7 Sketches of the wake of a plunging airfoil for various values of *kh*.

is inclined at an angle pointing upward and downstream relative to the neutral position of the airfoil. This phenomenon, classified as the dual mode, has also been observed by Dohring et al.[14] and Jones et al.[23] In fact, sometimes the vortex street could be formed such that it is inclined at an angle pointing downward relative to the neutral position of the airfoil. As found by Jones et al.,[25] the panel and Navier–Stokes calculations of a plunging airfoil show that the mode (that is, whether the vortex street is deflected upward or downward) is determined by the starting condition of the plunging oscillation.

Sketches of the vortex patterns as observed in Figs. 3–5 and in the video for various values of kh corresponding to drag-producing, neutral and thrust-producing, and dual-mode conditions are illustrated in Figs. 7a–7e, respectively.

B. Contours of Mean Streamwise Velocity

Figures 8a–8c display the contours of the nondimensional mean streamwise velocity $(U - U_0)/U_0$ for a NACA 0012 100-mm chord plunging airfoil for a freestream velocity of approximately 0.05 m/s. These contours have been smoothed by simply averaging neighboring points. The amplitude of oscillation is kept constant at $h = 0.06$ while the frequencies of oscillation are varied from 2.5, 5, to 10 Hz. These conditions correspond to kh of 1.762, 3.570, and 5.88, respectively. The flowfield displayed extends from $x/c = 0.5$ to 3 downstream of the trailing edge and exhibits all of the characteristics of a two-dimensional jet. The maximum jet velocity at $x/c = 0.5$ from the trailing edge of the plunging airfoil exceeds the freestream velocity by as much as 2.5–6.5 times when kh is increased from 1.762 to 5.88.

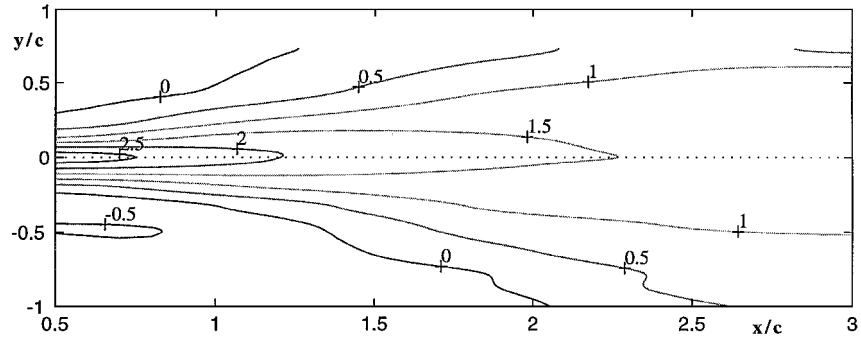

a) f = 2.5 Hz, h = 0.06, U_0 = 0.054 m/s (k = 29.36, kh = 1.76)

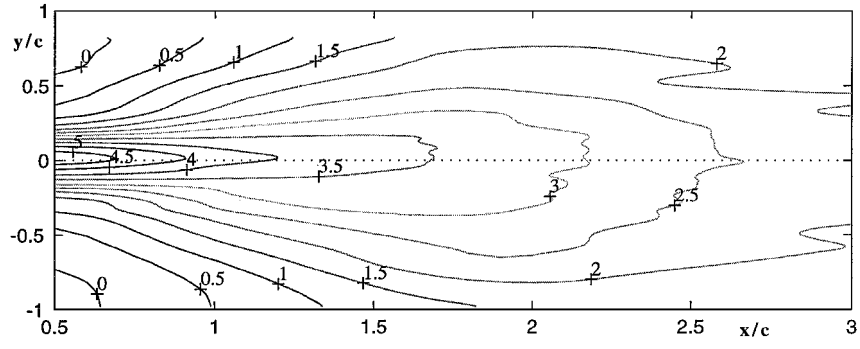

b) f = 5 Hz, h = 0.06, U_0 = 0.053 m/s (k = 59.50, kh = 3.57)

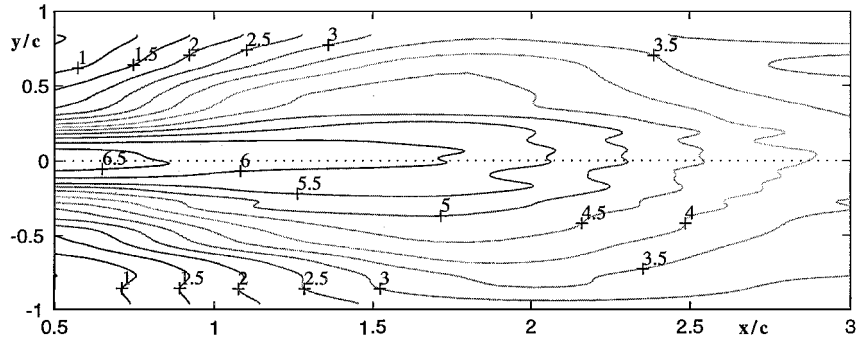

c) f = 10 Hz, h = 0.06, U_0 = 0.064 m/s (k = 98.02, kh = 5.88)

Fig. 8 Contours of nondimensional mean streamwise velocity $(U - U_0)/U_0$ for a 100-mm chord NACA 0012 airfoil oscillated in plunge.

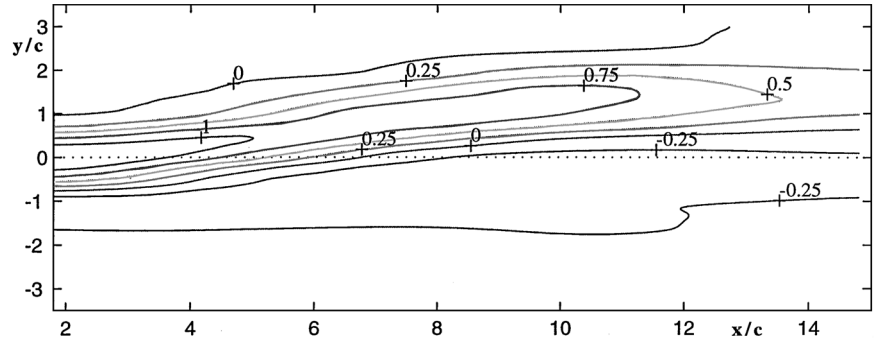

a) $f = 2.5$ Hz, $h = 0.6$, $U_0 = 0.053$ m/s ($k = 2.97$, $kh = 1.78$)

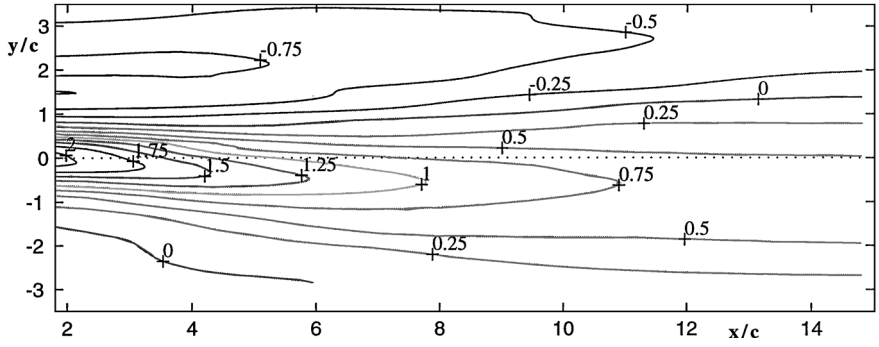

b) $f = 5$ Hz, $h = 0.6$, $U_0 = 0.052$ m/s ($k = 6.10$, $kh = 3.66$)

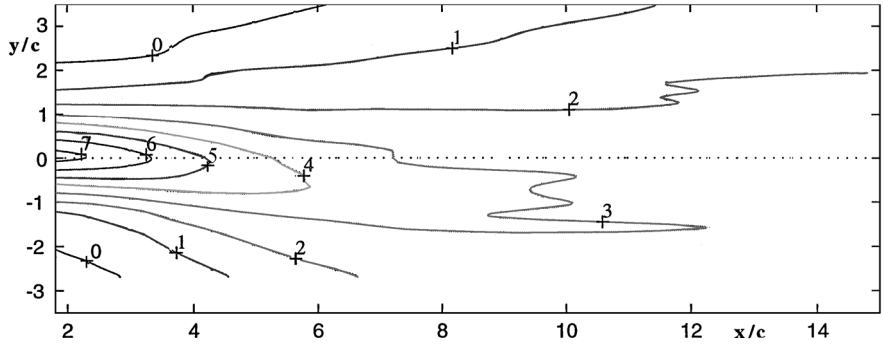

c) $f = 10$ Hz, $h = 0.6$, $U_0 = 0.040$ m/s ($k = 15.55$, $kh = 9.33$)

Fig. 9 Contours of nondimensional mean streamwise velocity $(U - U_0)/U_0$ for a 10-mm chord NACA 0012 airfoil oscillated in plunge.

Figures 9a–9c display the contours of the nondimensional mean streamwise velocity $(U - U_0)/U_0$ for a NACA 0012 10-mm chord plunging airfoil for a freestream velocity of approximately 0.05 m/s. The amplitude of oscillation is kept constant at $h = 0.6$ while three frequencies of oscillation are varied from 2.5, 5 to 10 Hz. These conditions correspond to kh of 1.78, 3.66, and 9.33, respectively. The flowfield displayed extends from $x/c = 1.8$ to 15 downstream of the trailing edge. Although a strong two-dimensional jet can be identified, a region where the mean streamwise velocity is less than the freestream velocity (i.e., drag-producing wake) can also be identified. Nevertheless, the spatial extent of thrust-producing jet far exceeds that of drag-producing wake. The mean streamwise velocity contours show that the jet is deflected either upward (Fig. 9a) or downward (Figs. 9b and 9c), thus exhibiting the behavior of the dual mode identified by Jones et al.[23] for kh greater than 1. The deflection of the jet is not as obvious in the near field close to the trailing edge (i.e., for $-1 < y/c < 1$ and $x/c < 3$). This is the reason why the contours in Figs. 8a–8c for the large airfoil with values of kh similar to Figs. 9 appear to be rather symmetrical because only the near field has been measured.

C. Streamwise Velocity Profiles

To further illustrate the jet produced by oscillating an airfoil in plunge, measured mean streamwise velocities in excess of the freestream velocity $(U - U_0)$ are nondimensionalized using $(U_{\max} - U_0)$, and the lateral coordinate y is nondimensionalized using the averaged jet half width b. Typical nondimensional streamwise velocity profiles $(U - U_0)/(U_{\max} - U_0)$ at various downstream stations are plotted against $(y - y_{\max})/b$ for two different amplitudes of oscillation, $h = 0.25$ and 0.4 in Figs. 10a and 10b, respectively. The frequency of oscillation is 10 Hz. In Fig. 10a the three different freestream velocities are $U_0 = 0.0532, 0.109$, and 0.22 m/s, resulting in $kh = 2.95$, 1.44, and 0.71, respectively. In Fig. 10b the three different freestream velocities are $U_0 = 0.0557$, 0.109, and 0.219 m/s, resulting in $kh = 4.51, 2.31$, and 1.15, respectively. Although a wake component can be seen on either side of the plane through $y = y_{\max}$ in both Figs. 10a and 10b, these profiles display the prominent jet nature of oscillating an airfoil in plunge. For some freestream conditions (such as $U_0 = 0.109$ m/s in Fig. 10a), the wake component appears above $y = 0$, but for other conditions (such as $U_0 = 0.22$ m/s in Fig. 10a) it appears below $y = 0$. These results indicate the dual-mode nature of the jet for $kh > 1$. Furthermore, there appears to be a reasonable collapse of the data using the freestream velocity as the velocity scale and the averaged jet half width as the length scale.

D. Maximum Streamwise Velocities

To quantify the effect of oscillating an airfoil in plunge, the maximum streamwise velocity at each downstream station for all the various tested flow conditions has been extracted from data such as those displayed in Figs. 9. The maximum streamwise velocity

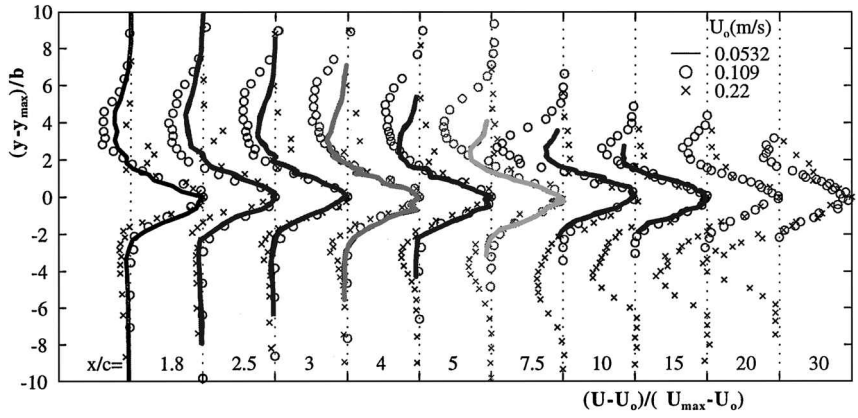

a) $f = 10$ Hz, $h = 0.25$ ($kh = 0.71, 1.44, 2.95$)

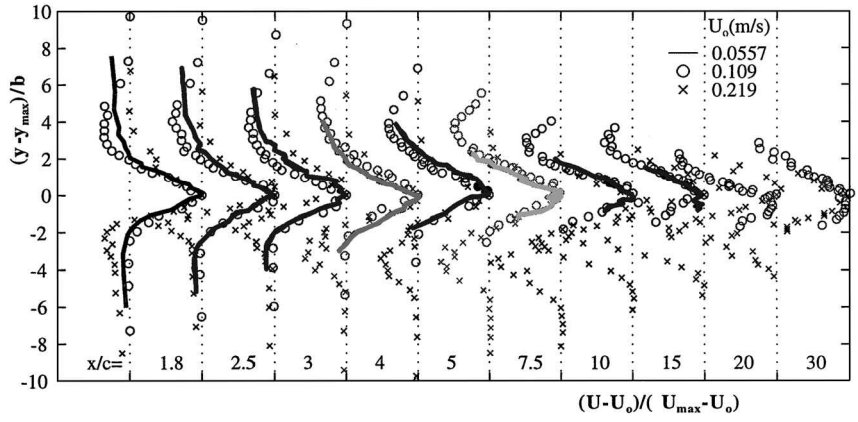

b) $f = 10$ Hz, $h = 0.4$ ($kh = 1.15, 2.31, 4.51$)

Fig. 10 Nondimensional streamwise velocity profiles for a 10-mm chord NACA 0012 airfoil.

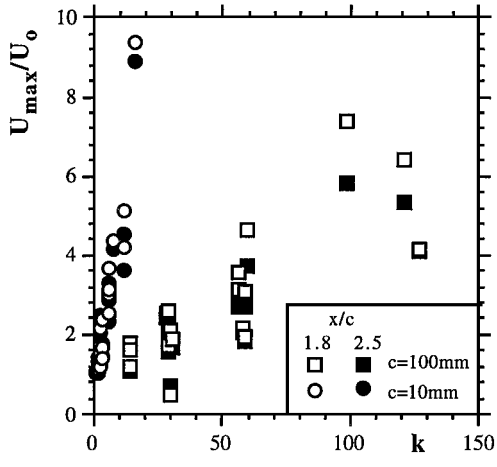

Fig. 11 Variation of U_{max}/U_0 with k.

U_{max}/U_0 obtained for $x/c = 1.8$ and 2.5 are plotted against the reduced frequency parameter k in Fig. 11 for the two different airfoil sizes. For the small airfoil ($c = 10$ mm) the maximum jet velocity can be over nine times as large as the freestream velocity at a reduced frequency of about 20. On the other hand, for the large airfoil ($c = 100$ mm) the maximum jet velocity at a reduced frequency of about 130 is about four times that of the freestream velocity. Obviously, the maximum streamwise velocity is dependent on both the reduced frequency k and the nondimensional amplitude of oscillation h. The data in Fig. 11 are replotted against the nondimensional plunge velocity kh in Figs. 12a and 12b for $x/c = 1.8$ and 2.5, respectively.

The data in Figs. 12a and 12b indicate that U_{max}/U_0 is now independent of the airfoil size and is a linear function of kh, with a correlation coefficient better than 0.98. These results thus indicate

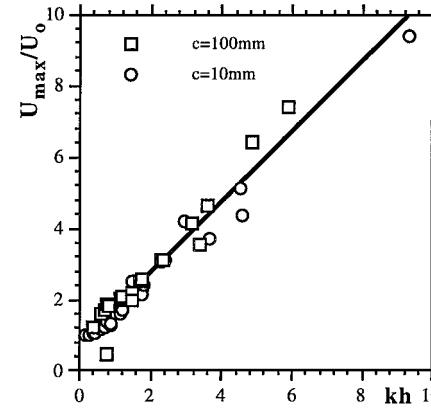

a) $x/c = 1.8$

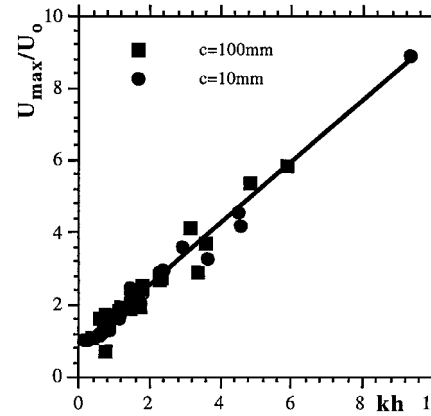

b) $x/c = 2.5$

Fig. 12 Variation of U_{max}/U_0 with kh.

that the nondimensional plunge velocity kh is the most relevant parameter in collapsing the maximum mean streamwise velocity data. The lines of best fit to the data shown in Figs. 12a and 12b are given, respectively, by

$$U_{\max}/U_0 = 0.981kh + 0.754 \quad \text{for} \quad x/c = 1.8 \tag{1}$$

$$U_{\max}/U_0 = 0.847kh + 0.80 \quad \text{for} \quad x/c = 2.5 \tag{2}$$

From Eqs. (1) and (2) one can estimate that the maximum mean streamwise velocity $U_{\max}$ is greater than the freestream velocity U_0 if kh is greater than 0.25. However, even if $U_{\max}$ is greater than U_0, there may not be net thrust produced because, as shown in Figs. 9 and 10, there is a wake component in the streamwise velocity profile. The errors involved in estimating thrust from time-averaged velocity profiles for flapping foils have been discussed in some depth by Streitlien and Triantafyllou.[26] Nevertheless, the mean streamwise velocity profiles such as those presented in Fig. 10 for various values of kh at $x/c = 15$ are integrated to provide an estimate of the thrust coefficient C_t. The variation of the experimentally determined thrust coefficient with kh is compared with that calculated by the linear analysis of Garrick[11] in Fig. 13. By assuming a nondeforming planar wake, the thrust coefficient C_t for a plunging airfoil is given by Garrick[11] as

$$C_t = 4\pi(kh)^2(F^2 + G^2) \tag{3}$$

where F and G are the real and imaginary parts of the Theodorsen lift deficiency function.

Figure 13 shows that for small values of kh (less than 1), there is reasonable agreement between the experimentally determined C_t and that calculated by Garrick.[11] For larger values of kh, the experimentally determined C_t is substantially less than that calculated by Garrick[11] because the thrust coefficient estimated from integration of mean streamwise velocity profiles would incur more errors and the linear analysis of Garrick[11] would not be valid for large kh. One can also see from the experimentally determined C_t that a net thrust is produced provided that kh is greater than 0.36. According to Anderson et al.,[21] optimum thrust production occurs for $0.8 \leq kh \leq 1.3$.

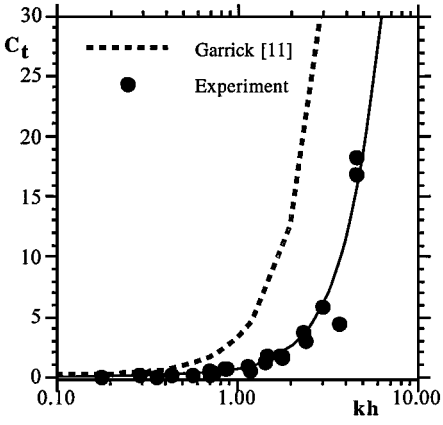

Fig. 13 Variation of thrust coefficient with kh.

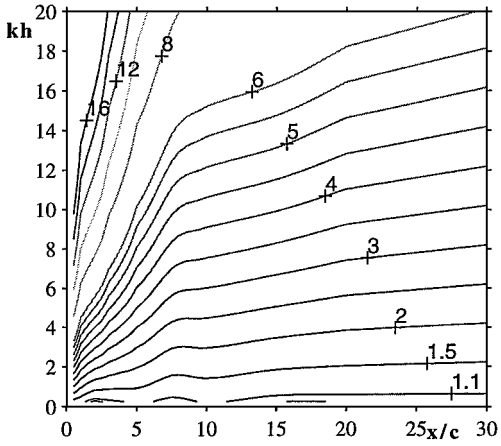

Fig. 14 Contours of nondimensional maximum streamwise velocity $U_{\max}/U_0$.

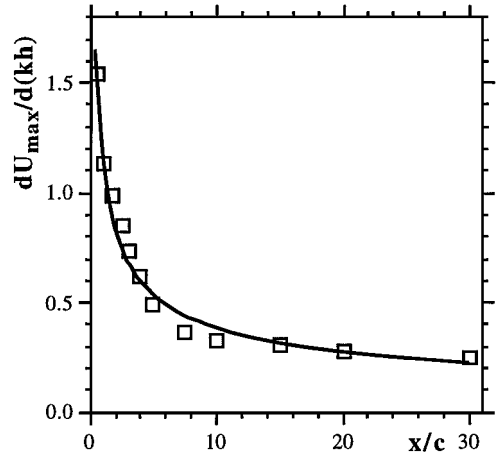

Fig. 15 Variation of $dU_{\max}/d(kh)$ with x/c.

E. Maximum Streamwise Velocity Decay

By fitting all of the $U_{\max}/U_0$ data at each x/c using a linear function of kh, contours of $U_{\max}/U_0$ as a function of x/c and kh can be obtained, as displayed in Fig. 14. These contours show that $U_{\max}$ for a given kh decreases as x/c increases, and at a given x/c it increases with kh. Figure 15 shows that $dU_{\max}/d(kh)$ varies approximately as $(x/c)^{-0.5}$, thus indicating that it behaves almost like a two-dimensional turbulent jet.

IV. Conclusions

The mean streamwise velocity field downstream of a NACA 0012 airfoil oscillated in plunge has been measured using a single-component LDV system and documented for a range of freestream velocities, frequencies, and amplitudes of oscillation. Dye flow visualization results show that the vortex patterns of a plunging airfoil change from drag producing at values of the nondimensional plunge velocity (kh) less than 0.2 to thrust-producing when kh is greater than approximately 0.4. LDV measurements of the mean streamwise velocity field show that a jet instead of a wake is produced downstream of a plunging airfoil for sufficiently high values of kh. The nondimensional plunge velocity has been shown to be an appropriate parameter to collapse the maximum streamwise velocity data for a total of 54 different test conditions covering a range of kh from 0.18 to 9.3. The estimation has been made that when kh is greater than 0.25 the maximum mean streamwise velocity is greater than the freestream velocity. Furthermore, the thrust coefficient estimated from the integration of mean streamwise velocity profiles increases with kh and is positive for kh greater than 0.36.

Acknowledgments

This work has been supported by the Office of Naval Research (Project Monitor E. Rood). Partial support from the Naval Postgraduate School provided under the National Research Council Research Associateship program to the first author while on leave from the Australian Defence Force Academy is gratefully acknowledged.

References

[1]Birnbaum, W., "Das ebene Problem des Schlagenden Fluegels," *Zeitschrift fuer Angewandte Mathematik und Mechanik*, Vol. 4, No. 4, 1924, pp. 277–292.

[2]Theodorsen, T., "General Theory of Aerodynamic Instability and the Mechanism of Flutter," NACA TR-496, May 1940.

[3]Ho, C. M., and Chen, S. H., "Unsteady Wake of a Plunging Airfoil," *AIAA Journal*, Vol. 19, No. 10, 1981, pp. 1492–1494.

[4]Ahmed, S., and Chandrasekhara, M. S., "Reattachment Studies of an Oscillating Airfoil Dynamic Stall Flowfield," *AIAA Journal*, Vol. 32, No. 5, 1994, pp. 1006–1012.

[5]Panda, J., and Zaman, K. B. M. Q., "Experimental Investigation of the Flow Field of an Oscillating Airfoil and Estimation of Lift from Wake Surveys," *Journal of Fluid Mechanics*, Vol. 265, 1994, pp. 65–95.

[6]Oshima, H., and Ramaprian, B. R., "Velocity Measurements over a Pitching Airfoil," *AIAA Journal*, Vol. 35, No. 1, 1997, pp. 119–126.

[7]Koochesfahani, M. M., "Vortical Patterns in the Wake of an Oscillating Airfoil," *AIAA Journal*, Vol. 27, No. 9, 1989, pp. 1200–1205.

[8]Knoller, R., "Die Gesetze des Luftwiderstandes," *Flug- und Motortechnik (Wien)*, Vol. 3, No. 21, 1909, pp. 1–7.

[9]Betz, A., "Ein Beitrag zur Erklaerung des Segelfluges," *Zeitschrift für Flugtechnik und Motorluftschiffahrt*, Vol. 3, No. 21, 1912, pp. 269–272.

[10]Katzmayr, R., "Effect of Periodic Changes of Angle of Attack on Behaviour of Airfoils," NACA TM 147, Oct. 1922.

[11]Garrick, I. E., "Propulsion of a Flapping and Oscillating Airfoil," NACA Rept. 567, May 1936.

[12]Schmidt, W., "Der Wellpropeller, ein neuer Antrieb fur Wasser-, Land-, und Luftfahrzeuge," *Zeitschrift für Flugwissenschaften*, Vol. 13, No. 12, 1965, pp. 472–479.

[13]Bosch, H., "Interfering Airfoils in Two-Dimensional Unsteady Incompressible Flow," *Unsteady Aerodynamics*, CP-227, AGARD, 1977, pp. 7-1–7-15.

[14]Dohring, C. M., Platzer, M. F., Jones, K. D., and Tuncer, I. H., "Computational and Experimental Investigation of the Wakes Shed from Flapping Airfoils and Their Wake Interference/Impingement Characteristic," *Characterisation and Modification of Wakes from Lifting Vehicles in Fluids*, CP-584, AGARD, 1996, pp. 33-1–33-9.

[15]Lai, J. C. S., Yue, J., and Platzer, M. F., "Control of Backward Facing Step Flow Using a Flapping Airfoil," *Proceedings of ASME Fluids Engineering Division* [CD-Rom], FEDSM97-3307, American Society of Mechanical Engineers, New York, 1997.

[16]Lighthill, M. J., "Note on the Swimming of Slender Fish," *Journal of Fluid Mechanics*, Vol. 9, 1960, pp. 305–317.

[17]Wu, Y. T., "Swimming of a Waving Plate," *Journal of Fluid Mechanics*, Vol. 10, 1961, pp. 21–344.

[18]Lan, C. E., "The Unsteady Quasi-Vortex-Lattice Method with Applications to Animal Propulsion," *Journal of Fluid Mechanics*, Vol. 93, 1979, pp. 747–765.

[19]Cheng, J. Y., Zhuang, L. X., and Tong, B. G., "Analysis of Swimming Three-Dimensional Waving Plates," *Journal of Fluid Mechanics*, Vol. 232, 1991, pp. 341–355.

[20]Triantafyllou, G. S., Triantafyllou, M. S., and Grosenbaugh, M. A., "Optimal Thrust Development in Oscillating Foils with Application to Fish Propulsion," *Journal of Fluids and Structures*, Vol. 7, No. 2, 1993, pp. 205–224.

[21]Anderson, J. M., Streitlien, K., Barrett, D. S., and Triantafyllou, M. S., "Oscillating Foils of High Propulsive Efficiency," *Journal of Fluid Mechanics*, Vol. 360, 1998, pp. 41–72.

[22]Freymuth, P., "Propulsive Vortical Signatures of Plunging and Pitching Airfoils," *AIAA Journal*, Vol. 26, No. 7, 1988, pp. 881–883.

[23]Jones, K. D., Dohring, C. M., and Platzer, M. F., "Experimental and Computational Investigation of the Knoller-Betz Effect," *AIAA Journal*, Vol. 36, No. 7, 1998, pp. 1240–1246.

[24]Dohring, C. M., "Experimental Analysis of the Wake of an Oscillating Airfoil," M.S. Thesis, Dept. of Aeronautics and Astronautics, Naval Postgraduate School, Monterey, CA, June 1996.

[25]Jones, K. D., Dohring, C. M., and Platzer, M. P., "Wake Structures Behind Plunging Airfoils: A Comparison of Numerical and Experimental Results," AIAA Paper 96-0078, Jan. 1996.

[26]Streitlien, K., and Triantafyllou, G. S., "On Thrust Estimates for Flapping Foils," *Journal of Fluids and Structures*, Vol. 12, No. 1, 1998, pp. 47–55.

P. R. Bandyopadhyay
Associate Editor

Color reproductions courtesy of the Naval Postgraduate School.